JOURNAL OF SOLID STATE CHEMISTRY **131,** 138–143 (1997)
ARTICLE NO. SC977366

Verwey-Type Transition and Magnetic Properties of the $LiMn_2O_4$ Spinels

Y. Shimakawa,*,[1] T. Numata,† and J. Tabuchi†

*Fundamental Research Laboratories, NEC Corporation, 34 Miyukigaoka, Tsukuba 305, Japan; and †Material Development Center, NEC Corporation, 4-1-1 Miyazaki, Miyamae-ku, Kawasaki 216, Japan

Received October 23, 1996; in revised form February 25, 1997; accepted February 27, 1997

The transport and magnetic properties of stoichiometric and Li-rich $LiMn_2O_4$ spinels are investigated. Clear anomalies, which are associated with a structural phase transition from cubic to tetragonal, are observed in the temperature dependence of resistivity and susceptibility in the stoichiometric sample. The sharp increase in resistivity with decreasing temperature suggests a transition similar to the Verwey transition seen in the Fe_3O_4 spinel. Electrical conduction above the transition temperature is well described by a hopping model with an activation energy of about 0.16 eV. Effective paramagnetic moments obtained from Curie constants yield information on the average ionic valence of Mn. The average ionic valences of Mn increase in the Li-rich samples, suggesting that the excess Li ions substitute on the Mn site. A superexchange magnetic interaction between the Mn ions *via* oxygen atoms is also discussed. The magnetic interaction in a 90° arrangement of Mn–O–Mn changes from antiferromagnetic to ferromagnetic with increasing Mn^{4+}/Mn^{3+} ratio. © 1997 Academic Press

INTRODUCTION

Lithium manganate spinel, $LiMn_2O_4$, is one of the most prominent materials used as cathode for rechargeable lithium batteries (1, 2). In the $LiMn_2O_4$ spinel structure, oxygen ions form a cubic-close-packed lattice, and Li and Mn ions are located at tetrahedral (8*a*) and octahedral (16*d*) sites, respectively. Electrochemical extraction of Li ions from the tetrahedral site occurs at 4 V, associated with the phase change of $LiMn_2O_4$ (average Mn valence, +3.5) to λ-MnO_2 (+4). Insertion of Li into the $LiMn_2O_4$ compound, on the other hand, occurs at 3 V, and causes a phase transition to $Li_2Mn_2O_4$ (+3). These three compounds have spinel-type structures, and thus the structural framework is kept intact by the extraction/insertion process of Li ions. The reduced $Li_2Mn_2O_4$ material shows tetragonal symmetry ($c/a \sim 1.16$) due to the Jahn–Teller distortion of $Mn^{3+}O_6^{2-}$ octahedra (1), whereas λ-MnO_2 has a cubic lattice ($c/a = 1$). Although the $LiMn_2O_4$ compound shows cubic symmetry at room temperature, the 50% concentration of Jahn–Teller Mn^{3+} ions is very close to the critical value of the structural transition between tetragonal and cubic lattices. Consequently, decreasing the temperature causes a structural phase transition around 280 K (3).

A problem to overcome for commercial applications of the $LiMn_2O_4$ spinel is poor cyclability of the charge–discharge process in the 4-V region. This should be considered as relating to the lattice instability of $LiMn_2O_4$ with the critical concentration of Mn^{3+} ions. Extensive studies on the exploration of high performance (high capacity and reliable cyclability and so on) cathode materials have shed light on nonstoichiometric phases in the vicinity of the stoichiometric composition of $LiMn_2O_4$. Recently, Gummow *et al.* reported that materials synthesized from Li-rich compositions showed significantly improved cyclability in the 4-V region (4). Yamada investigated a series of materials with Li-rich compositions and revealed that a small amount of excess Li suppressed the structural distortion (5). They suspected that the substitution of Li^{1+} ions on the Mn site, i.e., $Li(Li_xMn_{2-x})O_4$, increased the average ionic valence of Mn, thus decreasing the number of Jahn–Teller Mn^{3+} ions.

This paper describes transport and magnetic properties of stoichiometric and Li-rich $LiMn_2O_4$ spinels. Resistivity measurement reveals that phase transition in the stoichiometric sample has similarities to the Verwey transition seen in the Fe_3O_4 spinel (6, 7). Effective paramagnetic moments obtained from Curie constants provide the average ionic valence of Mn. The result of the increased Mn valence strongly suggests that the excess Li ions substitute on the Mn site in the Li-rich samples. Effects of Li/Mn ratios on the structure and a superexchange-type magnetic interaction are also discussed.

[1] To whom correspondence should be addressed.

0022-4596/97 $25.00
Copyright © 1997 by Academic Press
All rights of reproduction in any form reserved.

EXPERIMENTAL

Stoichiometric and Li-rich $LiMn_2O_4$ powder samples were synthesized by solid-state reaction. Mixtures of Li_2CO_3 and MnO_2 (EMD) with Li/Mn ratios ($\alpha/2$) of 1.00/2.00 (stoichiometric), 1.05/2.00, and 1.10/2.00 were calcined at 400°C for 8 h and then sintered at 750–900°C for 8 h in an oxygen atmosphere with intermediate grindings. The samples were confirmed to be single phase by X-ray diffraction using a conventional θ–2θ scanning method. Lattice constants were determined by a full-profile fit of X-ray diffraction data using the Rietveld analysis program RIETAN (8). Low temperature X-ray diffraction measurements from 300 to 25 K were carried out to confirm the structural phase transition.

Resistivity of the $\alpha = 1.00$ and 1.10 samples was measured by a four-probe method over the temperature range from 220 to 550 K with heating and cooling rates less than 0.5 K/min in 1 atm of air. Rectangular bars with the size of about $3(W) \times 3(H) \times 10(L)$ mm of the polycrystalline samples were used.

Magnetic properties were measured with a SQUID magnetometer. The temperature dependence of susceptibility was measured at temperatures decreasing from 380 to 5 K at an applied magnetic field of 5 T. M–H behaviors were also measured at 5 K in a magnetic field ranging from -5 to 5 T.

RESULTS AND DISCUSSION

The crystal structures of the samples at 300 K are of the cubic-spinel type with a space group of $Fd\bar{3}m$. Since the sintering temperature is relatively low, the X-ray diffraction peaks show isotropic and anisotropic broadening due to the small particle size and crystal strain. A full-profile fit using the Rietveld analysis gives precise lattice constants for the phases, and the results are listed in Table 1. The lattice constant decreases with increasing Li concentration α.

TABLE 1

Cubic Lattice Constant, Curie Constant (C), Weiss Temperature (θ), Obtained Mn^{3+}/Mn^{4+} Ratio, and Average Ionic Valence of Mn for the $LiMn_2O_4$ Spinels with Various α Values (Li/Mn = α/2.00)

α	1.00	1.05	1.10
a (Å)	8.2402	8.2338	8.2168
C (emu K/Mn-mol)	2.44	2.27	2.12
θ (K)	−315	−262	−202
Mn^{3+}/Mn^{4+}	0.50/0.50	0.35/0.65	0.22/0.78
Average Mn valence	+3.50	+3.65	+3.78

Figure 1 shows the temperature dependence of resistivity in the $\alpha = 1.00$ and 1.10 samples. With decreasing temperature, the resistivity in the $\alpha = 1.00$ sample increases nearly an order of magnitude at 290 K. This change in resistivity shows a temperature hysteresis of about 12 K, suggesting a first-order transition. In the $\alpha = 1.10$ sample, in contrast, no such anomaly is observed. The temperature dependence of resistivity in the $\alpha = 1.10$ sample shows a monotonic semiconductor-like behavior and is quite similar to the behavior observed in the $\alpha = 1.00$ sample above the transition temperature.

A clear anomaly can also be observed in the magnetic measurement. Figure 2 shows the temperature dependence of susceptibility (χ) and inverse susceptibility ($1/\chi$) in the $\alpha = 1.00$, 1.05, and 1.10 samples. With careful observation, a slight change in the slope of $1/\chi$ in the $\alpha = 1.00$ sample below about 290 K can be noticed. This is obvious in the plot of the derivative for $1/\chi$ versus temperature, shown in Fig. 3. An abrupt change in $d(1/\chi)/dT$ at 290 K in the stoichiometric sample can be observed.

These anomalies in resistivity and susceptibility in the stoichiometric sample should be related to a structural phase transition. X-ray diffraction peaks in Fig. 4 clearly show the phase transition. Bragg peaks of (4 4 0) [$2\theta \sim 44°$] and (3 3 3) and (5 1 1) [$2\theta \sim 58°$] in the cubic structure are observed in the $\alpha = 1.00$ and 1.10 samples at 300 K. At 250 K satellite peaks are seen in the $\alpha = 1.00$ sample, while no significant change is observed in the $\alpha = 1.10$ sample. The same results were first reported by Yamada *et al.* (3) and they assigned these satellite peaks as originating from a tetragonal phase with a space group of $I4_1/amd$. The phase transition temperatures of the stoichiometric sample determined from X-ray diffraction measurements are between

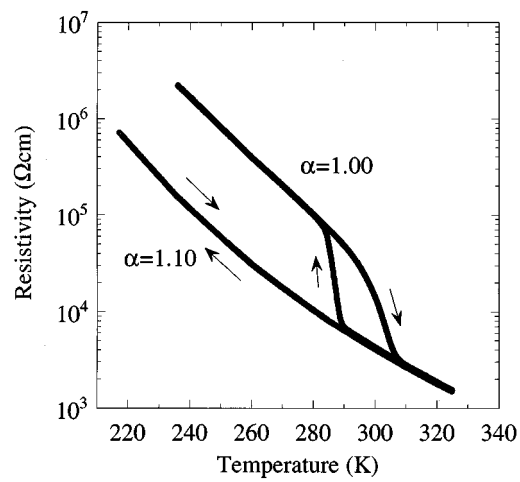

FIG. 1. Temperature dependence of resistivity for stoichiometric ($\alpha = 1.00$) and Li-rich ($\alpha = 1.10$) samples. Arrows in the figure indicate the results of changing the temperature.

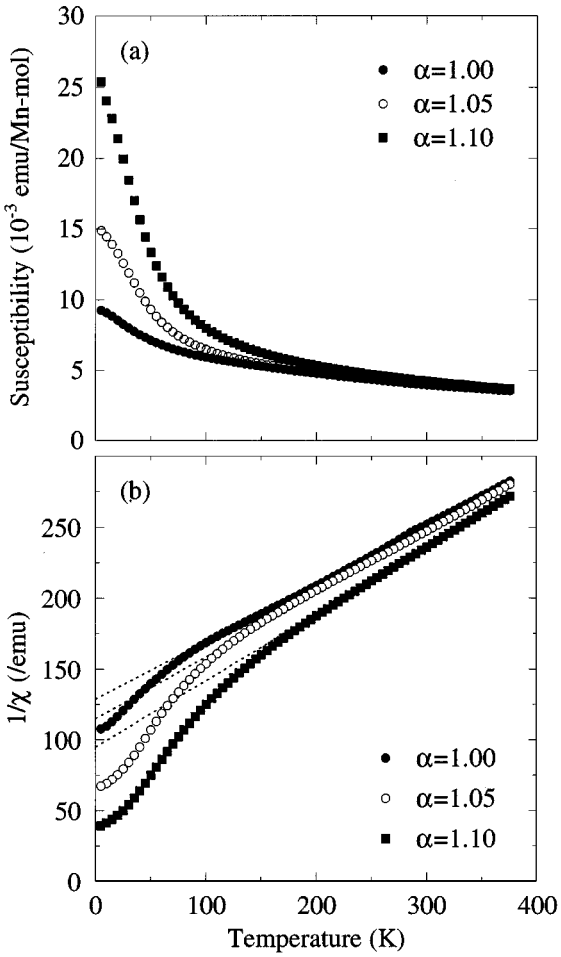

FIG. 2. Temperature dependence of (a) susceptibility and (b) inverse susceptibility for $\alpha = 1.00$, 1.05, and 1.10 samples. The results of the Curie–Weiss fit are also shown in (b) (see text).

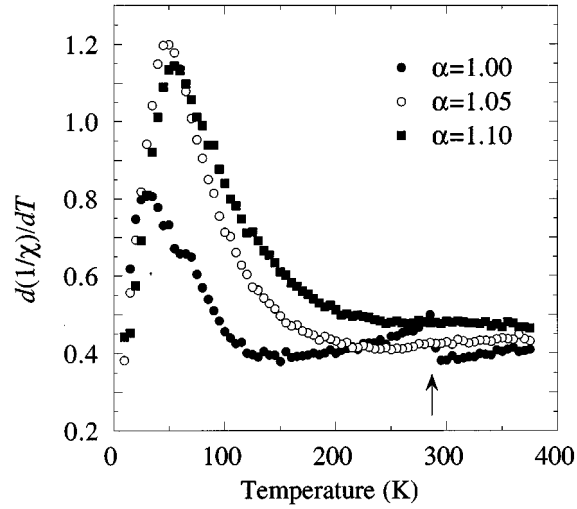

FIG. 3. Derivatives of inverse susceptibility, $d(1/\chi)/dT$, for $\alpha = 1.00$, 1.05, and 1.10 samples are plotted against temperature. The arrow indicates the phase transition (290 K) seen in the stoichiometric $\alpha = 1.00$ sample.

290 and 280 K with decreasing temperature and 300 and 310 K with increasing temperature. This agrees well with the results of resistivity measurement and also the results of differential scanning calorimetry (DSC) measurement by Yamada *et al.* (3). The fact that the present $\alpha = 1.05$ and 1.10 samples show no anomalous change in resistivity and susceptibility is consistent with the observation by Yamada; the DSC peaks corresponding to the phase transition smeared out in the $Li(Li_{0.035}Mn_{1.965})O_4$ sample (Li/Mn = 1.0356/2.00) (5).

The drastic change in resistivity at 290 K in the $\alpha = 1.00$ sample associated with the structural phase transition shows similarities to the Verwey transition in the Fe_3O_4 spinel. In Fe_3O_4 $[Fe^{3+}_{8a}(Fe^{2+}, Fe^{3+})_{16d}O_4]$ resistivity changes nearly two orders of magnitude at 125 K with the structural phase transition from a high-temperature cubic phase to a low-temperature low-symmetry phase. Although a satisfactory explanation for this transition has not yet been offered, models based on charge-ordering and polaron-ordering, for example, were proposed to describe the change in resistivity. Above the transition temperature, electron exchange between Fe^{2+} and Fe^{3+} ions at the octahedral site is responsible for high conductivity. The localization of electrons or the ordering of small polarons is believed to cause the increase in resistivity at the Verwey transition temperature (6, 7). In a stoichiometric $LiMn_2O_4$ spinel the octahedral site is occupied by Mn^{3+} and Mn^{4+} ions with the ratio of 1:1. Thus, similar charge-ordering between Mn^{3+} and Mn^{4+} ions could occur at the structural phase transition temperature. Since Mn^{3+} ions are Jahn–Teller ions, polaron-type conduction due to a strong electron–phonon interaction is expected. If this is the case, the ordering of small polarons could play an important role in the transition.

The conductivity at room temperature in the cubic $LiMn_2O_4$ spinels ($\sim 10^{-4}$ S/cm) is far lower than that in Fe_3O_4 ($\sim 10^2$ S/cm). Thus, electron exchange between Mn^{3+} and Mn^{4+} occurs less frequently and conductivity σ is well described by a hopping conduction model. In the model, conductivity σ as a function of temperature is described as

$$\sigma = (A/T)\exp(-E_h/kT), \qquad [1]$$

where A is a constant term including the concentration of hopping ions, E_h is hopping activation energy, and k is the Boltzmann constant (6). As shown in Fig. 5, where σT in a logarithmic scale is plotted against $1/T$, $\log(\sigma T)$ in the $\alpha = 1.00$ sample above the transition temperature and that

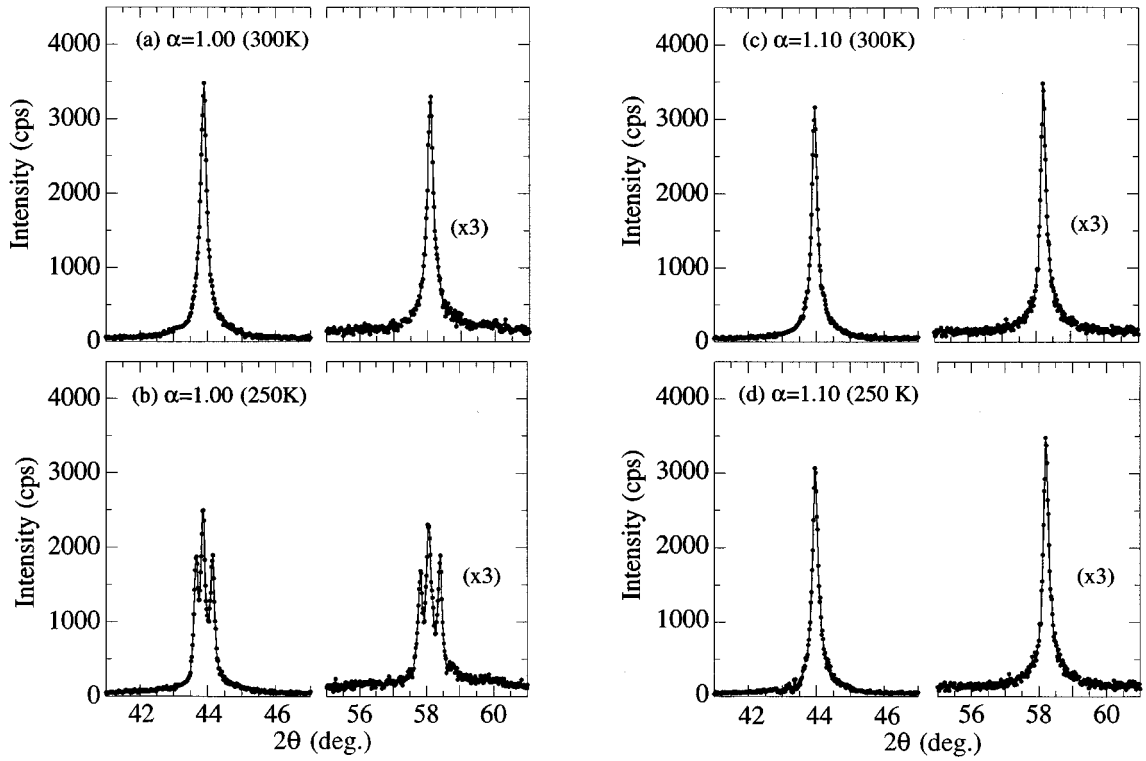

FIG. 4. X-ray diffraction peaks of (a) $\alpha = 1.00$ sample at 300 K, (b) $\alpha = 1.00$ sample at 250 K, (c) $\alpha = 1.10$ sample at 300 K, and (d) $\alpha = 1.10$ sample at 250 K. The $2\theta \sim 44^\circ$ Bragg peak is indexed as (4 4 0) in the cubic structure, and the $2\theta \sim 58^\circ$ peak as (3 3 3) and (5 5 1). Diffraction peaks by Cu$K\alpha_2$ X-ray have been subtracted from the observed profile.

in the $\alpha = 1.10$ sample for the measured temperature region obey this relationship. The obtained hopping activation energy is 0.16 eV, which is a typical value for thermally activated hopping conduction. Accordingly, a possible charge ordering of Mn^{3+}–Mn^{4+} ions from the disordered hopping state could cause a change in resistivity in the stoichiometric $LiMn_2O_4$ spinel. If the conduction in $LiMn_2O_4$ results from the hopping of small polarons, the resistivity change at 290 K could be explained by the order–disorder transition of small polarons.

In the stoichiometric $\alpha = 1.00$ sample, conductivity below the transition temperature also seems to obey Eq. [1] of the hopping model with almost the same activation energy. This may be explained by the coexistence of cubic and tetragonal phases at low temperatures as shown in Fig. 4. Yamada *et al.* reported that the volume fraction of the low-temperature tetragonal phase was 65% and that no single phase sample was obtained at 220 K (3). If the "intrinsic conductivity" of the low-temperature tetragonal phase is much lower than that of the high-temperature cubic phase, the observed conductivity below the transition temperature (two-phase region) mainly reflects the nature of the "unchanged cubic phase."

From the magnetic behaviors shown in Fig. 3, $d(1/\chi)/dT$ in the $\alpha = 1.00$ sample above the transition temperature and those in the $\alpha = 1.05$ and 1.10 samples above 200 K show constant values. Therefore, the susceptibility shown in Fig. 2 for each temperature range can be fitted by the Curie–Weiss law

$$\chi = C/(T - \theta). \qquad [2]$$

The obtained Curie constant (C) and Weiss temperature (θ) from a least squares fit are listed in Table 1. The results of Curie–Weiss fits and their extrapolated lines are also shown in Fig. 2. With increasing α, the Curie constant decreases, indicating a decrease in effective paramagnetic moment (P_{eff}). In the paramagnetic region, the Curie constant is written as

$$C = N_S P_{\text{eff}}^2 \mu_B^2 / 3k, \qquad [3]$$

where N_S and μ_B are the number of ions and the Bohr magneton, respectively. If we assume that only the spin part of the Mn ions contributes to paramagnetic moment and that the moment is a sum of the effective paramagnetic

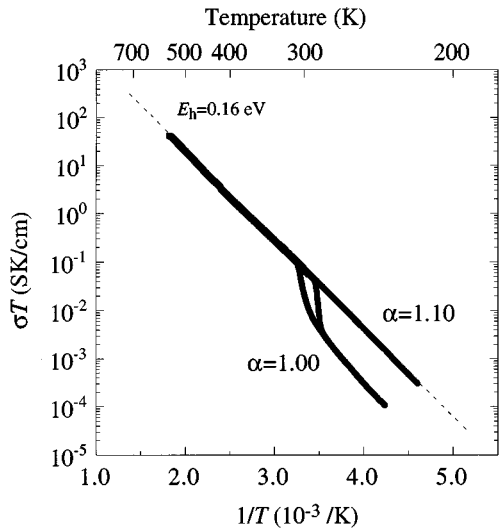

FIG. 5. σT in a logarithmic scale for $\alpha = 1.00$ and 1.10 samples are plotted against $1/T$. The results of a least squares fit to Eq. [1] are indicated by the dotted line.

moments of Mn^{3+} with high spin configuration ($S = 2$, 4.90 μ_B) and Mn^{4+} ($S = 3/2$, 3.87 μ_B) with a ratio of $y:(1-y)$, the Curie constant can be described as

$$C = N_S\{y4.90^2 + (1-y)3.87^2\}\mu_B^2/3k. \qquad [4]$$

Using this equation, the ratios Mn^{3+}/Mn^{4+} of the samples can be estimated. These results are also listed in Table 1.

The obtained ionic valence of Mn, +3.50, in the stoichiometric sample is equal to the expected value from the $Li^{1+}(Mn^{3+}, Mn^{4+})O_4^{2-}$ composition. The magnetic data clearly indicate the increase in the average ionic valence of Mn with increasing α. If the excess Li ions in the Li-rich materials are located at interstitial sites as expressed $Li_{1+x}Mn_2O_4$, the ionic valence of Mn is expected to decrease as α increases. The present results for increased Mn valences in the Li-rich compositions strongly suggest that the Li ions substitute for Mn at the octahedral site. The substitution of Li for Mn is also supported by a recent observation by Numata *et al.*, where density of samples measured by a pycnometer with helium gas decreased with increasing α (9). This behavior of decreasing density is quite similar to the change expected if we assume Li substitution on the octahedral Mn site. In a simple substitution model without vacancy, i.e., $Li(Li_xMn_{2-x})O_4$, the average valence of Mn is $(7-x)/(2-x)$. In this model, the $\alpha = 1.05$ and 1.10 samples can be written as $Li(Li_{0.033}Mn_{1.967})O_4$ and $Li(Li_{0.065}Mn_{1.935})O_4$ and the valences of Mn are expected to be +3.55 and +3.58, respectively. The valences of Mn obtained from magnetic measurements are slightly higher than the values expected from the simple model. A possible explanation to reconcile this discrepancy is a cation-vacancy model, i.e., $Li_{1-\delta}V_\delta(Li_xMn_{2-x-\eta}V_\eta)O_4$, where V represents the vacancy. This model is plausible because $Li_2Mn_4O_9$ is known to be a "defect spinel" described as $Li_{0.89}V_{0.11}(Mn_{1.78}V_{0.22})O_4$ (4, 10). The possibility of overestimating Mn valences, however, cannot be ruled out. The orbital moment of Mn 3*d* electrons may contribute to the effective paramagnetic moment. The effect of hybridization of the Mn 3*d* and O 2*p* orbitals could be included in the observed paramagnetic moment.

In the $\alpha = 1.05$ and 1.10 samples, the average Mn valences are greater than +3.5, i.e., the ratios of Jahn–Teller Mn^{3+} ions are less than 50%. Considering that these samples show no anomalies in resistivity and susceptibility, the transition from cubic to tetragonal phase, which is associated with cooperative Jahn–Teller structural distortions, should be suppressed in samples with higher Mn valences. The decrease in lattice constant with increasing α can also be explained by the change of the Mn^{3+}/Mn^{4+} ratio. Since the ionic radius of Mn^{4+} (0.530 Å (11)) octahedrally coordinated to oxygen ions is smaller than that of Mn^{3+} (0.645 Å for the high spin state (11)), the decrease of the Mn^{3+}/Mn^{4+} ratio should cause a decrease in the spinel lattice. Although substitution of Li^{1+} (0.76 Å for the octahedral coordination (11)) for smaller Mn ions causes counter behavior, the number of produced Mn^{4+} ions is larger than the number of substituting Li^{1+} ions. Thus, the "average ionic size" of the octahedral site decreases with increasing α.

The Weiss temperatures of the three samples are negative, indicating antiferromagnetic interaction between the Mn spins. With increasing α, however, the extrapolated Weiss temperatures increase, which suggests that antiferromagnetic interaction decreases in the samples with a higher valence state of Mn. As shown in Fig. 6, ferromagnetic components are seen in *M–H* behaviors at low temperature in the $\alpha = 1.05$ and 1.10 samples, while *M* changes linearly with *H* in the $\alpha = 1.00$ sample. As has been discussed by Goodenough, superexchange interaction in a nearly 90° arrangement of the Mn–O–Mn bond strongly depends on the electron configuration of the cation (6). Ferromagnetic interaction is usual in the Mn^{4+}–O–Mn^{4+} bond, while antiferromagnetic interaction is expected in Mn^{3+}–O–Mn^{3+} and Mn^{3+}–O–Mn^{4+}. Therefore, with increasing concentration of Mn^{4+} ions in the system, the ferromagnetic component is dominant against antiferromagnetic interaction. Tabuchi *et al.* recently reported similar results on a series of defect spinels $Li_{1-\delta}Mn_{2-2\delta}O_4$ (12). Masquelier *et al.* also reported positive Weiss temperature of the $Li_4Mn_5O_{12}$ spinel [$Li(Li_{0.33}Mn_{1.67})O_4$ with an average Mn valence of +4] (13). All these observations suggest a crossover from antiferromagnetic to ferromagnetic interaction in the samples with high Mn valences.

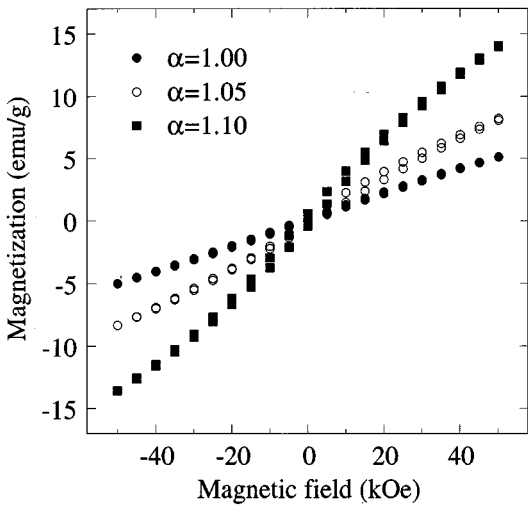

FIG. 6. *M–H* behaviors at 5 K for $\alpha = 1.00$, 1.05, and 1.10 samples.

CONCLUSION

$LiMn_2O_4$ spinels, which will be useful as cathode for rechargeable lithium batteries, were investigated from the viewpoint of transport and magnetic properties. The stoichiometric $LiMn_2O_4$ sample showed clear anomalies at 290 K in resistivity and susceptibility, which were associated with the structural phase transition from cubic to tetragonal. This transition has similarities to the Verwey transition seen in the Fe_3O_4 spinel. Although the conduction mechanism for the $LiMn_2O_4$ spinel has not been clarified, a hopping conduction model with an activation energy of about 0.16 eV explained the resistivity behavior for the high-temperature cubic phase. The observed paramagnetic moments were the sum of the effective moments of Mn^{3+} and Mn^{4+} and provided average ionic valences of Mn. The average Mn valences increased with increasing excess Li composition, suggesting Li^{1+} substitution on the Mn site. The structural phase transition was suppressed in samples with higher Mn valences ($> +3.5$). Superexchange magnetic interaction in the 90° arrangement of Mn–O–Mn changed from antiferromagnetic to ferromagnetic with increasing Mn^{4+}/Mn^{3+} ratio, as suggested by changes in Weiss temperature and *M–H* behavior.

The present results do not provide any direct information on the performance of battery cells with $LiMn_2O_4$ cathodes. However, there were many differences in the physical properties between the stoichiometric $LiMn_2O_4$ sample (which usually shows poor cyclability in the 4-V region) and the Li-rich samples (which show better battery performance). The insertion/extraction process of Li ions in the $LiMn_2O_4$ spinel might be affected by the natures of parent spinel materials such as crystal structures and average Mn valences.

ACKNOWLEDGMENTS

The authors thank Dr. Kubo for helpful discussion. They also thank Mr. Tomioka and Mr. Kumeuchi for preparing the samples.

REFERENCES

1. M. M. Thackeray, W. I. F. David, P. G. Bruce, and J. B. Goodenough, *Mater. Res. Bull.* **18,** 461 (1983).
2. M. M. Thackeray, P. J. Johnson, L. A. de Picciotto, P. G. Bruce, and J. B. Goodenough, *Mater. Res. Bull.* **19,** 179 (1984).
3. A. Yamada and M. Tanaka, *Mater. Res. Bull.* **30,** 715 (1995).
4. R. J. Gummow, A. de Kock, and M. M. Thackeray, *Solid State Ionics* **69,** 59 (1994).
5. A. Yamada, *J. Solid State Chem.* **122,** 160 (1996).
6. J. B. Goodenough, *in* "Progress in Solid State Chemistry" (H. Reiss, Ed.), Vol. 5, p. 145. Pergamon Press, Oxford, 1971.
7. N. Tsuda, K. Nasu, A. Yanase, and K. Siratori, *in* "Electronic Conduction in Oxides," Vol. 94, p. 207. Springer-Verlag, Berlin, 1991.
8. F. Izumi, *in* "The Rietveld Method" (R. A. Young, Ed.), p. 236. Oxford Univ. Press, Oxford, 1993.
9. T. Numata, J. Tabuchi, T. Kumeuchi, U. von Sacken, J. N. Reimers, and Q. Zhong, "Proc. of The 190th Meeting of The Electrochemical Society, 1996," p. 1014.
10. A. de Kock, M. H. Rossouw, L. A. de Picciotto, M. M. Thackeray, W. I. F. David, and R. M. Ibberson, *Mater. Res. Bull.* **25,** 657 (1990).
11. R. D. Shannon, *Acta Crystallogr. A* **32,** 751 (1976).
12. M. Tabuchi, C. Masquelier, H. Kobayashi, R. Kanno, Y. Kobayashi, T. Akai, Y. Maki, H. Kageyama, and O. Nakamura, preprint, 1996.
13. C. Masquelier, M. Tabuchi, K. Ado, R. Kanno, Y. Kobayashi, Y. Maki, O. Nakamura, and J. B. Goodenough, *J. Solid State Chem.* **123,** 255 (1996).